

NC-REG : NEURAL CORTICAL MAPS FOR RIGID REGISTRATION

*Ines Vatti^{1,2}, Pierrick Bourgeat¹, Rodrigo Santa Cruz², Vincent Dore¹,
Olivier Salvado², Clinton Fookes², Léo Lebrat²*

¹ CSIRO, Australia

²Queensland University of Technology, Australia

ABSTRACT

We introduce *neural cortical maps*, a continuous and compact neural representation for cortical feature maps, as an alternative to traditional discrete structures such as grids and meshes. It can learn from meshes of arbitrary size and provide learnt features at any resolution. *Neural cortical maps* enable efficient optimization on the sphere and achieve runtimes up to 30 times faster than classic barycentric interpolation (for the same number of iterations). As a proof of concept, we investigate rigid registration of cortical surfaces and propose NC-Reg, a novel iterative algorithm that involves the use of *neural cortical feature maps*, gradient descent optimization and a *simulated annealing* strategy. Through ablation studies and subject-to-template experiments, our method demonstrates sub-degree accuracy (< 1° from the global optimum), and serves as a promising robust pre-alignment strategy, which is critical in clinical settings.

Index Terms— Spherical registration, Cortical surface, Deep learning, 3D Rotations, Global optimization

1. INTRODUCTION AND RELATED WORK

Accurate cortical surface Non-Rigid Registration (NRR) is crucial for comparing brain anatomy across subjects, enabling population studies and clinical applications. The main drawbacks of existing NRR methods are the intricate processing of spherical meshes, commonly used to model the brain cortex [1], and a strong reliance on an accurate initial rigid alignment.

For example, Spherical Demons (SD) [2], which achieves competitive runtimes compared to FreeSurfer (FS) [1] (which takes approximately 30 minutes for spherical registration [3, 4]), performs rotation searches at each multi-resolution level. Hierarchical Spherical Deformation (HSD) [5] jointly optimizes global rigid alignment and local deformation using spherical harmonics, ensuring smooth transformations. Those multi-resolution, iterative approaches achieve high accuracy but remain slow. Even faster deep learning-based methods still rely on error-prone remeshing and rigid pre-alignment. For instance, S3Reg [6] requires substantial computational resources (especially during training) to enable their proposed convolution and pooling operations on meshes, and performs

rigid registration via exhaustive angle searches similarly to SD and FS. Other methods, such as DDR [7], GeoMorph [3] and SUGAR [4], integrate rotation prediction within their models, but they often lack generalization when spherical meshes are largely misaligned.

As previously noted, most neuroimaging pipelines, including FS [1], ANTs [8], and BrainSuite [9], represent the cortical surface as discrete triangular meshes composed of vertices, edges, and faces. Typical cortical meshes contain about 140,000 vertices per hemisphere. To reduce computational complexity, most approaches downsample these high-resolution surfaces to regular icosahedral meshes [10], then upsample the final deformation using Thin Plate Spline interpolation (e.g., MSM [11]) or linear interpolation (e.g., SD [2]). Classical optimization on discrete meshes requires barycentric interpolation at each iteration to warp the moving surface, which is computationally intensive and error-prone. A common workaround is to project surface features onto 2D images for interpolation, but this introduces distortions. Large surface regions can map to sub-pixel areas [12], ultimately degrading accuracy. To address these limitations, learning-based representations have emerged in computer vision as continuous and compact alternatives to discrete structures. Yang et al. [13] explored geometric processing on *neural implicit fields*, deep networks predicting signed distance functions. *Overfitted* neural networks (NN), i.e. trained on a single surface, have also been proposed [12], leveraging the universal approximation theorem [14]. More recently, Williamson et al. [15] introduced geometric processing tools operating directly on Spherical Neural Surfaces (SNS), exploiting the smooth, differentiable nature of neural networks to model genus-0 surfaces without remeshing. DeepCSR [16] predicted implicit surface representations of the brain cortex, but *overfitted* neural models remain under-explored in neuroimaging.

Inspired by neural radiance fields (NeRF) [17], we propose *Neural Cortical maps* (NC), a continuous and compact representation for modeling cortical feature maps. Our NN takes coordinates on the sphere as input and outputs features of interest. Once trained on a mesh of arbitrary size, the model can provide features at any cortical location without mesh interpolation. To demonstrate its practical utility, we propose NC-Reg, a novel rotational registration method using

NC, and a *Simulated Annealing* (SA) strategy [18]. We show that NC-Reg is efficient, fast and accurate. It is also a robust pre-alignment strategy that enhances downstream NRR performance. Our contributions are (1) a novel neural representation for cortical maps that trains easily on meshes of any size and generates features on meshes at arbitrary resolutions, (2) a fast iterative algorithm for global rigid registration on the sphere, and (3) a robust initialization strategy for NRR.

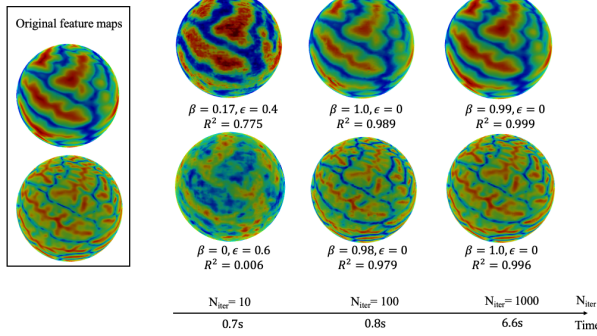


Fig. 1: Learning two cortical feature maps using different numbers of training iterations (N_{iter}). To evaluate cortical feature reconstruction, we realised a linear regression between the interpolated values and the model outputs for an icosahedron of level 6 (40,962 vertices). β is the slope, ϵ the intercept, and R^2 the coefficient of determination. The NN recovers both large-scale geometric features (average convexity, top) and high-frequency features (mean curvature, bottom).

2. METHOD

2.1. Definition and Training of Neural Cortical Maps

We are interested in learning a continuous representation of cortical surfaces. We define a Multi-Layer Perceptron (MLP) parametrized by φ , referred to as a *neural cortical map* (NC), $\mathcal{S}_\varphi : \mathbb{S}^2 \rightarrow \mathbb{R}^{n_f}$, where \mathbb{S}^2 is the 2-dimensional unit sphere and n_f is an arbitrary number of features (e.g., mean curvature, convexity, sulcal depth and/or cortical thickness). The input p of this neural network is a point lying on the unit sphere $p \in \mathbb{S}^2$. The input is further encoded using a multiresolution hash encoding [19]. The deep learning model outputs the feature values at p . In practice, its architecture is the fast fully-fused MLP¹ from [20].

Let $\mathcal{G} = (\mathcal{V}, \mathcal{F})$ be the original spherical mesh where \mathcal{V} is the set of vertices and \mathcal{F} is the set of faces. The map $\mathbf{f} : \mathcal{V} \rightarrow \mathbb{R}^{n_f}$ gives the feature values for a given vertex. At each training step, we sample n_F faces on the original mesh \mathcal{G} and n_V random points on each sampled face. Let $p_1, p_2, p_3 \in \mathcal{V}$ be the vertices of the sampled face. A sampled point is obtained by $p = ap_1 + bp_2 + cp_3$ where (a, b, c)

are random scalars in the standard 2-simplex Δ^2 . The target feature values of a random point p is obtained via barycentric interpolation

$$I(p) = \frac{|p_2 p_3 p| \mathbf{f}(p_1) + |p_1 p_3 p| \mathbf{f}(p_2) + |p_1 p_2 p| \mathbf{f}(p_3)}{|p_2 p_3 p| + |p_1 p_3 p| + |p_1 p_2 p|} \quad (1)$$

where $|p_i p_j p|$ is the area of the triangle $[p_i, p_j, p]$.

A gradient descent approach is performed to optimize the network parameters φ using Adam optimizer [21] that minimizes a feature matching energy such as the Mean Squared Error (MSE) between S_φ and I .

Figure 1 shows some results of the training on a given subject. The representation can also be seen as a compression for large meshes. For instance, a mesh of 136,804 vertices has a size of 4.57 MB and each feature file is 0.51 MB. The MLP would have about 3.7 MB (adding more output features changes only the last layer, which is negligible in terms of memory), while allowing for fast reconstruction of a subject’s cortical mesh for any resolution.

2.2. Global Rotational Registration Algorithm

Let $F : \mathbb{S}^2 \rightarrow \mathbb{R}^{n_f}$ be the fixed feature map and $M : \mathbb{S}^2 \rightarrow \mathbb{R}^{n_f}$ be the moving feature map. We aim at finding the optimal rotation $R \in SO(3)$ where $SO(3)$ is the Special Orthogonal group such that $RR^T = R^T R = I$ and $\det(R) = 1$ that solves $\min_{R \in SO(3)} \int_{\mathbb{S}^2} \mathcal{L}(F(p), M \circ R(p)) dp$. This integral is approximated by sampling N points on the sphere. The energy \mathcal{L}_t at iteration t for a rotation R_t reads

$$\mathcal{L}(F, M, R_t) = \frac{1}{N} \sum_{i=1}^N \text{MSE}(F(p_i) - M(R_t \cdot p_i)) \quad (2)$$

Minimizing Equation (2) is non convex and optimizing rotations is usually problematic, mainly because they are non-Euclidean in nature [22]. To handle the fact that many local minima exist, we propose a random exploration of the rotation space, i.e. every time the algorithm is “stuck” within a local minimum, a random resetting of the rotation parameters is proposed and the gradient descent starts from this new initialization. The resetting is either completely random (w/o SA) or subject to a certain acceptance probability (SA) as described in Algorithm 1.

Many rotation parametrizations exist. One can mention Euler angles, quaternions, and axis-angle parametrization. Zhou et al. [23] also introduced the continuous 6D representation for 3D rotations estimation. The rotation model is “reset” by converting a random axis-angle representation. The rotation angle is uniformly sampled in $[0, 2\pi]$ and the rotation axis is obtained by normalizing a Gaussian vector.

The moving average $\bar{\mathcal{L}}_t = \sum_{i=t-t_m}^{t-1} \mathcal{L}_i$ of the loss function (2) is computed at each iteration t . A local minima is identified when the difference $|\mathcal{L}_t - \bar{\mathcal{L}}_t|$ is below a certain threshold for a certain number of iterations t_{diff} . We keep the local minimum with the lowest validation loss.

¹<https://github.com/NVlabs/tiny-cuda-nn>

Algorithm 1 SA reset strategy. A temperature parameter T_t is decreased every time a local minimum is identified until a temperature minimum T_{\min} is reached. The idea is that when close to the end of the optimization, the probability of accepting a worse candidate is smaller. In practice, $T_{\min} = 10^{-4}$, $\alpha_T = 0.9$ ($0 < \alpha_T < 1$), $N_{T,\text{iter}} = 5$.

```

1: for  $k \in \llbracket 1, N_{T,\text{iter}} \rrbracket$  do
2:    $R_{\text{rand}} \sim \mathcal{U}(SO(3))$ 
3:    $\Delta \mathcal{L} = \mathcal{L}(\{p_i\}_1^N, F, M, R_{\text{rand}}) - \mathcal{L}_t$ 
4:   if  $\Delta \mathcal{L} < 0$  OR  $(\Delta \mathcal{L} > 0 \text{ and } \mathcal{U}([0, 1]) < \exp(-\frac{\Delta \mathcal{L}}{T_t}))$ 
    then
5:      $R_{t+1} \leftarrow R_{\text{rand}}$ 
6:     break
7:   end if
8: end for
9: if  $T_t > T_{\min}$  then
10:   $T_{t+1} \leftarrow \alpha_T T_t$ 
11: end if

```

3. EXPERIMENTS AND RESULTS

In Figure 1, after *overfitting* a subject from the ADNI dataset, a linear regression between model outputs and interpolated values of new vertices yields a near-identity function, confirming the fidelity of the learned representation. In the following, we focus on the spherical registration problem. We trained a NC model on the *fsaverage* template from FreeSurfer v7.4 over 3,000 iterations for about 18s.

We use the Washington University Alzheimer’s Disease Research Center (ADRC) dataset, which includes 39 cortical meshes with expert manual parcellations and compare the rigid and non-rigid alignment of each subject to the template. To assess robustness to initialization, we also created a *perturbed* dataset by applying random rotations to each cortical mesh: $(\text{roll}, \text{yaw}, \text{pitch}) \sim \mathcal{U}([-36^\circ, 36^\circ]^3)$. To evaluate the alignment quality, we compute the MSE and the Pearson Correlation Coefficient (PCC) for two cortical features: mean curvature (curv) and convexity (sulc). We also compute the Dice score of the template and registered subject parcellations. To compare two rotations $R_1, R_2 \in SO(3)$, we convert them to their quaternion representation ($q_1, q_2 \in \{q \in \mathbb{R}^4, \|q\|^2 = 1\}$) and compute the quaternion error as it is bi-invariant and respects the topology on $SO(3)$ [24]

$$\text{dist}_R(q_1, q_2) = \arccos(|q_1 \cdot q_2|) \in [0, \pi/2] \subset \mathbb{R}^+ \quad (3)$$

Experiments were performed on a NVIDIA H100 GPU, except for SD which was run in Matlab R2024b using fine-tuned parameters.

3.1. Rigid Registration - Ablation Study

As expected, increasing the number of iterations increases the chance of converging to the global optimum (Figure 2).

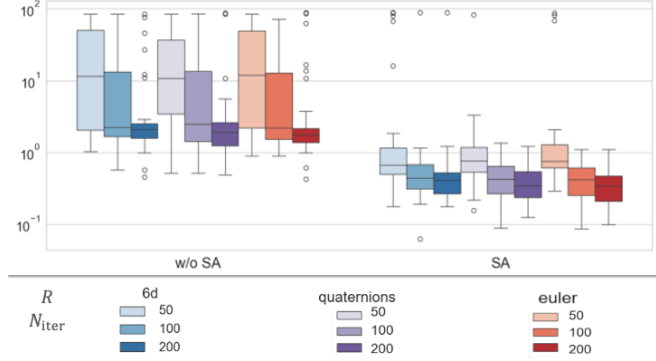


Fig. 2: Rotation distance $\text{dist}_R(R^*, R^*_{\text{perturbed}} \cdot R_{\text{rand}})$ in degrees (Equation (3)) between the solutions obtained on the same subject for two different initializations. For each subject, R^* is the optimized solution (for the default initialization). R_{rand} is the random perturbation applied to the subject mesh. $R^*_{\text{perturbed}}$ is the optimized solution to register the *perturbed* subject to the template.

Our algorithm shows strong robustness and consistency. With $N_{\text{iter}} \geq 100$, solutions from different initializations remain within 1° of each other. Although SA adds less than one second to runtime, it substantially improves feature alignment and ensures successful registration across all subjects (Table 1). The choice of rotation model showed no significant impact. In the following experiments, we use SA, quaternion model and $N_{\text{iter}} = 100$.

Table 1: Comparison of *reset* strategies for NC-Reg on the *perturbed* dataset. “Worst Dice” indicates the proportion of subjects for which the Dice score decreased after registration. Results use $N_{\text{iter}} = 200$ and quaternion parametrization as it yielded the best performance across all methods. Two-tailed paired-sample *t*-tests compare MSE, PCC and Dice values between SA and other strategies (${}^*p < 0.005$), with 95% confidence intervals shown.

Method	MSE (\downarrow)	PCC (\uparrow)	Dice (\uparrow)	Time (s)	Worst Dice
perturbed dataset					
w/o Reset	$0.156 \pm 0.030^*$	$0.403 \pm 0.067^*$	$0.559 \pm 0.096^*$	0.63 ± 0.002	6/39 (15.4%)
w/o SA	$0.125 \pm 0.015^*$	$0.454 \pm 0.037^*$	$0.677 \pm 0.055^*$	0.69 ± 0.008	2/39 (5.1%)
SA	0.098 ± 0.007	0.532 ± 0.021	0.761 ± 0.019	1.48 ± 0.01	0/39 (0.0%)

3.2. Robust Rigid Pre-Alignment

We benchmarked our rigid registration method against two state-of-the-art approaches: the pre-trained SUGAR model [4] and the CUDA implementation of HSD algorithm [5] for the first degree of freedom ($l = 0$, see Section 2.3 in [25]).

Table 2 shows that NC-Reg achieves comparable or superior performance to state-of-the-art methods. It significantly

Table 2: Comparison to registration baselines. Total time for SUGAR includes the time for interpolating the given subject mesh to the icosahedron of level 6 (before inputting it to the network) and the inference time. We performed two-tailed paired-sample t -tests between each rigid method and NC-Reg (* $p < 0.001$), between SD and NC-Reg+SD (• $p < 0.005$), and between SUGAR and NC-Reg+SUGAR († $p < 0.005$).

Method	MSE (↓)		PCC (↑)		Dice (↑)	Time (s)	Worst Dice
	curv	sulc	curv	sulc			
Rigid registration on the ADRC dataset							
NC-Reg (ours)	0.027 ± 0.0008	0.169 ± 0.014	0.328 ± 0.022	0.735 ± 0.021	0.761 ± 0.018	0.84 ± 0.01	0.0%
Interp-Reg	0.027 ± 0.0008	0.169 ± 0.014	0.329 ± 0.0215	0.735 ± 0.021	0.760 ± 0.018	48.67 ± 0.48	0.0%
Rigid SUGAR	0.028 ± 0.0010*	0.181 ± 0.016*	0.297 ± 0.0255*	0.716 ± 0.024*	0.760 ± 0.014	1.55 ± 0.07	0.0%
Rigid HSD (ico4)	0.027 ± 0.0008	0.168 ± 0.013*	0.327 ± 0.0213	0.738 ± 0.021*	0.760 ± 0.017	5.98 ± 0.08	0.0%
Rigid HSD (ico6)	0.027 ± 0.0009	0.167 ± 0.013*	0.329 ± 0.0218	0.738 ± 0.021*	0.761 ± 0.017	14.85 ± 0.39	0.0%
Rigid registration on the <i>perturbed</i> dataset							
NC-Reg (ours)	0.027 ± 0.0008	0.170 ± 0.014	0.327 ± 0.022	0.734 ± 0.021	0.760 ± 0.018	0.79 ± 0.01	0.0%
Interp-Reg	0.028 ± 0.0011	0.193 ± 0.030	0.306 ± 0.0288	0.697 ± 0.048	0.715 ± 0.054	44.59 ± 1.59	5.1%
Rigid SUGAR	0.038 ± 0.0010*	0.508 ± 0.046*	0.043 ± 0.0247*	0.200 ± 0.072*	0.306 ± 0.066*	1.24 ± 0.05	12.8%
Rigid HSD (ico4)	0.027 ± 0.0009	0.167 ± 0.013*	0.328 ± 0.0218	0.738 ± 0.021*	0.760 ± 0.017	8.59 ± 0.26	0.0%
Non-rigid registration on the ADRC dataset							
SD	0.017 ± 0.0004	0.056 ± 0.003	0.580 ± 0.009	0.914 ± 0.004	0.820 ± 0.007	37.93 ± 0.47	0.0%
NC-Reg + SD	0.017 ± 0.0004	0.057 ± 0.004	0.581 ± 0.0098	0.913 ± 0.006	0.819 ± 0.008	31.70 ± 0.44	0.0%
SUGAR	0.018 ± 0.0004	0.062 ± 0.002	0.546 ± 0.008	0.905 ± 0.003	0.825 ± 0.006	1.79 ± 0.07	0.0%
NC-Reg + SUGAR	0.018 ± 0.0004	0.063 ± 0.003	0.545 ± 0.0090	0.903 ± 0.005	0.822 ± 0.009	2.40 ± 0.04	0.0%
HSD	0.019 ± 0.0004	0.066 ± 0.003	0.534 ± 0.008	0.900 ± 0.004	0.811 ± 0.007	17.28 ± 0.27	0.0%
Non-rigid registration on the <i>perturbed</i> dataset							
SD	0.017 ± 0.0004	0.057 ± 0.003	0.574 ± 0.010	0.912 ± 0.005	0.812 ± 0.008	35.55 ± 0.26	0.0%
NC-Reg + SD	0.017 ± 0.0004•	0.056 ± 0.003	0.582 ± 0.0091•	0.914 ± 0.004	0.821 ± 0.007•	30.26 ± 0.35	0.0%
SUGAR	0.025 ± 0.0012	0.167 ± 0.025	0.388 ± 0.031	0.731 ± 0.042	0.412 ± 0.089	1.46 ± 0.05	7.7%
NC-Reg + SUGAR	0.018 ± 0.0004†	0.063 ± 0.003†	0.545 ± 0.0089†	0.903 ± 0.005†	0.822 ± 0.009†	2.13 ± 0.05	0.0%
HSD	0.019 ± 0.0004	0.066 ± 0.003	0.534 ± 0.008	0.900 ± 0.004	0.811 ± 0.007	17.27 ± 0.30	0.0%

outperforms SUGAR on the *perturbed* datasets as deep-learning models usually do not generalize well. Rigid HSD runtime highly depends on the chosen resolution, while our approach is consistently faster.

For NRR, we replace the rigid component of SD and SUGAR with our rotational pre-alignment. We observed that replacing the rotation search in SD by the initialization obtained with NC-Reg decreases the time by about 5s and yields better Dice score for the *perturbed* dataset. Using NC-Reg pre-alignment drastically improves SUGAR results on the *perturbed* dataset. Overall, NC-Reg provides an efficient and reliable initialization, improving both rigid and non-rigid registration pipelines.

4. CONCLUSION AND DISCUSSION

We introduced NC maps, a new continuous representation for cortical feature maps, and demonstrated their utility in rigid registration. Our representation addresses key limitations of discrete representations by enabling differentiable optimization and reducing computational overhead. More specifically, this approach trains a model on a given template mesh of arbitrary size, and subsequently replaces mesh-based interpola-

tion with a simple forward pass through the pre-trained MLP. Surface registration experiments on the ADRC dataset show that our approach achieves accuracy comparable to state-of-the-art methods while being consistently faster and more robust to large rotations. Integrating our optimization-based rigid initialization improves Dice scores and robustness in existing pipelines. Because the template NC model only needs to be fit once, its small pre-training cost is negligible, and using it for registration provides a clear runtime and computational advantage over classic mesh representations.

Future work will include evaluating our method on the MindBoggle dataset with another set of features to assess its robustness. We also plan to integrate *neural cortical maps* into an end-to-end neuroimaging pipeline with automatic cortical feature computation and NC-based NRR methods for more efficient and scalable surface-based analysis.

5. COMPLIANCE WITH ETHICAL STANDARDS

This research study was conducted using human subject data made available in open access.

ADNI dataset can be found at adni.loni.usc.edu, and ADRC dataset at people.csail.mit.edu/ythomas/code_release.

6. REFERENCES

- [1] Bruce Fischl, “FreeSurfer,” *NeuroImage*, vol. 62, no. 2, pp. 774–781, Aug. 2012.
- [2] B.T. Thomas Yeo, et al., “Spherical Demons: Fast Diffeomorphic Landmark-Free Surface Registration,” *IEEE transactions on medical imaging*, vol. 29, no. 3, pp. 650–668, Mar. 2010.
- [3] Mohamed A. Suliman, et al., “GeoMorph: Geometric Deep Learning for Cortical Surface Registration,” in *Proceedings of the First International Workshop on Geometric Deep Learning in Medical Image Analysis*. Nov. 2022, pp. 118–129, PMLR, ISSN: 2640-3498.
- [4] Jianxun Ren, et al., “SUGAR: Spherical ultrafast graph attention framework for cortical surface registration,” *Medical Image Analysis*, vol. 94, pp. 103122, May 2024.
- [5] Ilwoo Lyu, et al., “Hierarchical spherical deformation for cortical surface registration,” *Medical Image Analysis*, vol. 57, pp. 72–88, Oct. 2019.
- [6] Fenqiang Zhao, et al., “S3reg: Superfast spherical surface registration based on deep learning,” *IEEE transactions on medical imaging*, vol. 40, no. 8, pp. 1964–1976, Aug. 2021.
- [7] Mohamed A. Suliman, et al., “A deep-discrete learning framework for spherical surface registration,” in *Medical Image Computing and Computer Assisted Intervention – MICCAI 2022*, Linwei Wang, et al., Eds. 2022, pp. 119–129, Springer Nature Switzerland.
- [8] Nicholas J. Tustison, et al., “Large-scale evaluation of ANTs and FreeSurfer cortical thickness measurements,” *NeuroImage*, vol. 99, pp. 166–179, Oct. 2014.
- [9] David W. Shattuck, et al., “BrainSuite: an automated cortical surface identification tool,” *Medical Image Analysis*, vol. 6, no. 2, pp. 129–142, June 2002.
- [10] Abdulah Fawaz, et al., “Benchmarking Geometric Deep Learning for Cortical Segmentation and Neurodevelopmental Phenotype Prediction,” Dec. 2021, bioRxiv.
- [11] E.C. Robinson, et al., “MSM: A new flexible framework for multimodal surface matching,” *NeuroImage*, vol. 100, pp. 414–426, 2014.
- [12] Luca Morreale, et al., “Neural Surface Maps,” in *2021 IEEE/CVF Conference on Computer Vision and Pattern Recognition (CVPR)*, June 2021, pp. 4637–4646, ISSN: 2575-7075.
- [13] Guandao Yang, “Geometry processing with neural fields,” in *SIGGRAPH Asia 2023 Doctoral Consortium*. Nov. 2023, pp. 1–5, ACM.
- [14] Kurt Hornik, et al., “Multilayer feedforward networks are universal approximators,” *Neural Networks*, vol. 2, no. 5, pp. 359–366, Jan. 1989.
- [15] R. Williamson, et al., “Neural geometry processing via spherical neural surfaces,” *Computer Graphics Forum*, 2025.
- [16] Rodrigo Santa Cruz, et al., “DeepCSR: A 3D Deep Learning Approach for Cortical Surface Reconstruction,” in *2021 IEEE Winter Conference on Applications of Computer Vision (WACV)*, Waikoloa, HI, USA, Jan. 2021, pp. 806–815, IEEE.
- [17] Ben Mildenhall, et al., “NeRF: Representing scenes as neural radiance fields for view synthesis,” Aug. 2020.
- [18] S. Kirkpatrick, et al., “Optimization by Simulated Annealing,” *Science*, vol. 220, no. 4598, pp. 671–680, May 1983, Publisher: American Association for the Advancement of Science.
- [19] Thomas Müller, et al., “Instant neural graphics primitives with a multiresolution hash encoding,” *ACM Transactions on Graphics*, vol. 41, no. 4, pp. 1–15, July 2022.
- [20] Thomas Müller, et al., “Real-time neural radiance caching for path tracing,” *ACM Trans. Graph.*, vol. 40, no. 4, pp. 36:1–36:16, July 2021.
- [21] Diederik Kingma, et al., “Adam: A method for stochastic optimization,” *International Conference on Learning Representations*, 12 2014.
- [22] F. Sebastian Grassia, “Practical Parameterization of Rotations Using the Exponential Map,” *Journal of Graphics Tools*, vol. 3, no. 3, pp. 29–48, Jan. 1998.
- [23] Yi Zhou, et al., “On the Continuity of Rotation Representations in Neural Networks,” in *2019 IEEE/CVF Conference on Computer Vision and Pattern Recognition (CVPR)*, Long Beach, CA, USA, June 2019, pp. 5738–5746, IEEE.
- [24] Du Q. Huynh, “Metrics for 3D Rotations: Comparison and Analysis,” *Journal of Mathematical Imaging and Vision*, vol. 35, no. 2, pp. 155–164, Oct. 2009.
- [25] Ilwoo Lyu, et al., “Hierarchical Spherical Deformation for Shape Correspondence,” in *Medical Image Computing and Computer Assisted Intervention – MICCAI 2018*. 2018, pp. 853–861, Springer International Publishing.